Available online at www.sciencedirect.com

SciVerse ScienceDirect

Magnetic Resonance Imaging 31 (2013) 212–220

MAGNETIC RESONANCE IMAGING

Signal fluctuations in fMRI data acquired with 2D-EPI and 3D-EPI at 7 Tesla

João Jorge [a, b, c], Patrícia Figueiredo [a, b,*], Wietske van der Zwaag [d], José P. Marques [d]

[a] Department of Bioengineering, Instituto Superior Técnico, Technical University of Lisbon, Lisbon, Portugal
[b] Institute for Systems and Robotics, Lisbon, Portugal
[c] Laboratory for Functional and Metabolic Imaging, École Polytechnique Fédérale de Lausanne, Lausanne, Switzerland
[d] Department of Radiology, Université de Lausanne, Lausanne, Switzerland

Received 17 February 2012; revised 30 April 2012; accepted 8 July 2012

Abstract

Segmented three-dimensional echo planar imaging (3D-EPI) provides higher image signal-to-noise ratio (SNR) than standard single-shot two-dimensional echo planar imaging (2D-EPI), but is more sensitive to physiological noise. The aim of this study was to compare physiological noise removal efficiency in single-shot 2D-EPI and segmented 3D-EPI acquired at 7 Tesla. Two approaches were investigated based either on physiological regressors (PR) derived from cardiac and respiratory phases, or on principal component analysis (PCA) using additional resting-state data. Results show that, prior to physiological noise removal, 2D-EPI data had higher temporal SNR (tSNR), while spatial SNR was higher in 3D-EPI. Blood oxygen level dependent (BOLD) sensitivity was similar for both methods. The PR-based approach allowed characterization of relative contributions from different noise sources, confirming significant increases in physiological noise from 2D to 3D prior to correction. Both physiological noise removal approaches produced significant increases in tSNR and BOLD sensitivity, and these increases were larger for 3D-EPI, resulting in higher BOLD sensitivity in the 3D-EPI than in the 2D-EPI data. The PCA-based approach was the most effective correction method, yielding higher tSNR values for 3D-EPI than for 2D-EPI postcorrection.

Keywords: Signal fluctuations; Physiological noise; Segmented 3D-EPI; BOLD fMRI; Ultra-high field

1. Introduction

High-field magnetic resonance imaging (MRI) provides considerable improvements in image signal-to-noise ratio (SNR) [1], potentially allowing for higher sensitivity and spatial resolution in blood oxygen level dependent (BOLD) functional MRI (fMRI). However, the increase of noise from non-thermal sources, including physiological processes as well as spontaneous neural activity and subject motion, imposes an asymptotic limit on the achievable temporal SNR (tSNR) [2–4]. Great effort has therefore been dedicated to the characterization and correction of physiological noise [5–11]. Several types of physiological signal fluctuations have been identified: (a) quasi-periodic signal oscillations due to the pulsatility of blood flow in the brain and magnetic field changes induced by respiratory motion [5]; (b) nonperiodic fluctuations due to low-frequency drifts in end-tidal CO_2 (a potent vasodilator), caused by subtle, naturally occurring changes in breathing rate and depth [6]; (c) nonperiodic fluctuations due to cross-beat changes in heart rate (affecting cerebral hemodynamics, namely, oxyhemoglobin concentration), which may occur in several frequency bands [7].

Besides the field strength, B_0, the noise characteristics of fMRI can be affected by imaging parameters such as the echo time (TE), the flip angle [4], the voxel volume [12] or the imaging sequence.

Commonly used two-dimensional echo planar imaging (2D-EPI) techniques tend to present increasingly longer single volume acquisition times at higher fields, as a result of the possibility of achieving higher spatial resolution. This is further encouraged by studies showing that physiological noise contributions can be minimized by reducing voxel size [13]. Furthermore, thinner slices have the advantage of reduced signal loss due to through-slice dephasing, but result in higher numbers of slices per volume for adequate coverage. Segmented three-dimensional EPI (3D-EPI) has recently been

* Corresponding author. Institute for Systems and Robotics, Department of Bioengineering, Instituto Superior Técnico, Universidade Técnica de Lisboa, Av. Rovisco Pais, 1, 1049-001 Lisboa, Portugal. Tel.: +351 218418277; fax: +351 218418291.
E-mail address: patricia.figueiredo@ist.utl.pt (P. Figueiredo).

0730-725X/$ – see front matter © 2013 Elsevier Inc. All rights reserved.
http://dx.doi.org/10.1016/j.mri.2012.07.001

proposed as a promising technique for high-resolution fMRI at ultra-high fields, in which one *k*-space plane is acquired after each excitation pulse [14]. When optimizing the signal using the Ernst angle, 3D-EPI offers superior image SNR relative to standard 2D-EPI due to the whole-volume radio-frequency (RF) excitations [14], which can be traded for higher spatial resolution and offer lower specific absorption rate (SAR) levels due to the smaller optimal flip angle [15]. More importantly, it allows parallel imaging acceleration in two spatial dimensions, significantly reducing total volume acquisition times. In 2D-EPI, acceleration in the slice-encoding direction can be achieved either by time multiplexing, in which case signals from different slices are refocused at different times within an EPI echo train [16], or by multislice simultaneous excitation, in which case the different slices are separated thanks to the varying coil profiles [17,18]. The first method has a penalty in terms of increased distortion artifacts (arising from the longer echo train needed), and as both methods rely on the excitation of an increased number of slices per unit of time, they have an SAR penalty that can make their use prohibitive at high field strengths. Despite the 3D-EPI advantages in terms of spatial SNR (sSNR), physiological noise contributions appear to increase in functional data, thus compromising potential tSNR increases [14,15,19]. This disadvantage becomes more important at ultra-high fields, given the above-mentioned dependence of physiological noise contributions on B_0 [2–4]. Several physiological noise removal strategies have been developed. One group relies on inclusion of physiological information in the general linear model (GLM), depending on assumptions regarding the influence of physiological processes on BOLD signals and requiring physiological data acquisition simultaneously with fMRI [5–7,9]. These methods are applicable to resting-state data as well as task-driven fMRI, and allow the characterization of physiological signal contributions. All three physiological noise components mentioned in the first paragraph can be separately modeled and removed with this methodology. Another powerful approach for task-driven fMRI involves the identification of physiological signal fluctuations with the aid of a separately acquired resting-state data set [10]. Here, all correlated signal fluctuations unrelated to the external stimulus are addressed simultaneously, including spontaneous signal fluctuations.

The present work aims to compare physiological noise characteristics in standard 2D-EPI and 3D-EPI data, acquired at 7 Tesla, and test physiological noise correction methods for BOLD fMRI. A physiological regressor (PR)-based approach [9] and a principal component analysis (PCA)-based approach [10] were applied to both data types.

2. Materials and methods

2.1. Data acquisition

Ten healthy subjects (aged 26±4 years, four males, six females) were studied, with approval from the institutional review board of the local ethics committee, and provided written informed consent. One subject was excluded from PR-based analyses due to corrupted physiological recordings, and a second subject was excluded from both PR-based and PCA-based analyses due to a lack of significant activation in 2D data.

Each subject underwent four fMRI runs, counterbalanced across subjects: rest with eyes closed (*Rest*), visual localizer paradigm (*Loc*) acquired with a 2D-EPI or a 3D-EPI sequence. The localizer paradigm consisted of the visual presentation of faces (*F*), houses (*H*), objects (*O*) and scrambled objects (*S*), separated by fixation periods, in a block design of 18s blocks [20,21].

MRI data were acquired using a 7 Tesla/680-mm scanner (Siemens Medical Solutions, Erlangen, Germany), with an eight-channel head array coil (RAPID Biomedical GmbH, Germany). For each fMRI run, 112 volumes were acquired from a region covering the primary and ventral visual cortex. Multislice single-shot 2D-EPI volumes consisted of 40 interleaved 2mm thick slices with a volume acquisition time of 3.2s (TR_{2D}/α_{2D}=3200ms/63°–65°). In segmented 3D-EPI, a seven-lobe *sinc* pulse was used to obtain a good slab selection profile; 40 *k*-space planes were sequentially encoded, with a single *k*-space segment measured after each RF excitation, followed by application of a crusher gradient, with a volume acquisition time of 3.2s (TR_{3D}/α_{3D}=80ms/18°). Although spurious echo formation is not a problem at TR=80ms [15], RF spoiling was also applied to avoid instability of the transverse steady-state magnetization [19]. The TE (25ms), parallel imaging acceleration factor (GeneRalized Autocalibrating Partially Parallel Acquisitions (GRAPPA)=2 for the in-plane phase-encoding direction), matrix size (104×104), field of view (210×210mm^2) and resolution (2mm isotropic) were kept the same for both techniques.

Whole-brain structural images for anatomical reference were acquired using the MP2RAGE sequence, a modified magnetization-prepared rapid gradient-echo (MPRAGE) sequence that generates two image sets at different inversion times for bias field compensation [22], with 1×1×1mm^3 spatial resolution. Single-volume whole-brain 2D-EPI images (104×104×80 voxels, 2×2×2mm^3 spatial resolution, TE=25ms, α_{2D}=65°) were acquired to aid spatial co-registration, providing more coverage and thus anatomical landmarks than the fMRI data sets.

Respiratory amplitude and pulse oximetry levels were recorded at a 50Hz sampling rate simultaneously with the fMRI acquisition, utilizing the respiratory belt and pulse oximeter provided with the MRI scanner.

2.2. MRI data analysis

Data analysis was performed with the FMRIB Software Library (FSL 4.1.2, http://www.fmrib.ox.ac.uk/fsl) and routines implemented in Matlab for the optimization steps (http://www.mathworks.com). Following a set of common preprocessing steps, two analysis approaches were employed for physiological noise characterization and correction: a PR-based [9] and a PCA-based [10] approach.

2.2.1. General processing steps

Using FSL, *Loc* and *Rest* functional images were co-registered, motion corrected, temporally high-pass filtered (300s cutoff period), slice timing corrected in the 2D case, smoothed (3mm Full Width at Half Maximum (FWHM) Gaussian) and normalized to the Montreal Neurological Institute (MNI) space. Data were subsequently analyzed with a conventional GLM regression approach [23]. GLM design matrices (DMs) included a base set, DM_0, with stimulus and slow drift regressors. For the *Loc* data analysis, this matrix comprised the four visual stimuli convolved with a standard hemodynamic response function, their temporal derivatives and a set of slow drift regressors to measure the contribution of drift components in the time courses. For the *Rest* data analysis, DM_0 contained only slow drift regressors. GLM analyses were followed by activation clustering, using a Z threshold of 2.3 and a cluster p threshold of 0.05 [24].

2.2.2. Region of interest (ROI) definition

Voxel-based results were averaged across subject- and acquisition type-specific ROIs: two active regions (ROI_{Act1} and ROI_{Act2}, Fig. 1), a gray matter region (ROI_{GM}), a white matter region (ROI_{WM}) and a background region (ROI_{BG}). For ROI_{Act1}, the global contrast $F+H+O+S$ vs. fixation ($FHOS>b$) was used to identify the visual cortex; for ROI_{Act2}, the more specific contrast F vs. $H+O+S$ ($F>HOS$) was used to identify cortical areas specifically responding to faces. ROI_{Act1} and ROI_{Act2} were determined as the binary intersection between a visual cortex mask and the $FHOS>b$ cluster, and the intersection of a ventral visual cortex mask with the $F>HOS$ cluster, respectively. While not mutually exclusive, these two functional activation ROIs correspond to different types of regions commonly detected in fMRI experiments: a more confined and an extended active region. They were considered in order to test the effectiveness of the correction approaches as a function of the spatial specificity of a given BOLD response. This is particularly important for high-resolution fMRI studies, which frequently seek very specific functional responses in small brain areas. ROI_{WM} and ROI_{BG} were defined as 8×8 voxel squares placed, respectively, in parietal white matter brain regions or outside the brain in regions not affected by Nyquist ghosting. Two reference ROIs (ROI_{Ref1} and ROI_{Ref2}), further described in Section 2.2.4, were used during PCA-based analyses and are also shown in Fig. 1.

2.2.3. PR-based analysis

The PR-based approach [9] involved the extraction of GLM regressors from physiological signal recordings. For each fMRI run, a second-order RETROICOR (Image-based method for retrospective correction of physiological motion effects in fMRI) regressor set, with a total of eight regressors [5,9], a single respiration volume per unit time (RVT) regressor [6] and a single cardiac rate (CR) regressor [7] were generated. Prior to regressor extraction, respiratory amplitude and pulse oximetry signal peak detection was done using a wavelet-based algorithm adapted from Ref. [25]. The temporal middle of the volume acquisition was used for definiton of the phases of the respiration and cardiac cycle in both the 2D-EPI and 3D-EPI data. Temporal shifts relative to the fMRI time courses were optimized for CR and RVT regressors in order to account for delay effects or feedback mechanisms involving blood CO_2 levels and respiratory rate as in Refs. [6,7]. The developed regressor sets were then selectively grouped with DM_0 in order to build six nested regression models for GLM analysis, as follows:

$$\begin{aligned} DM_1 &= [DM_0\ r_{RETRc}] \\ DM_2 &= [DM_0\ r_{RETRr}] \\ DM_3 &= [DM_0\ r_{RETR}] \\ DM_4 &= [DM_3\ r_{CR}] \\ DM_5 &= [DM_3\ r_{RVT}] \\ DM_6 &= [DM_3\ r_{CR}\ r_{RVT}] \end{aligned}, \qquad (1)$$

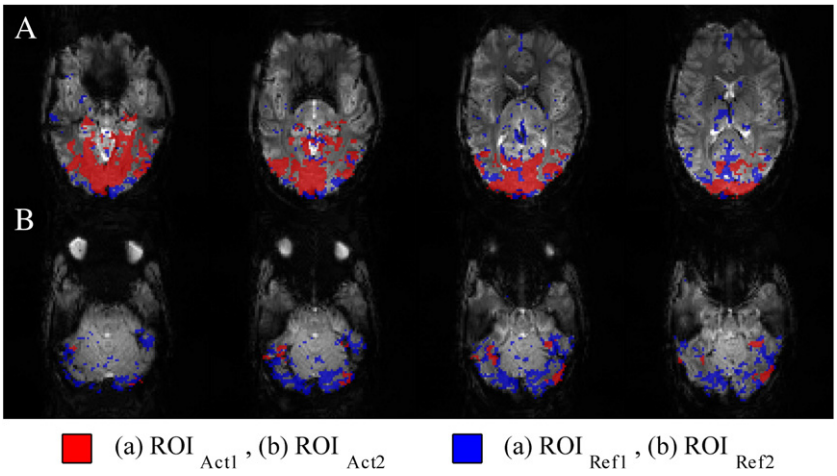

Fig. 1. Active and reference ROIs obtained for an example subject: (A) ROI_{Act1} (red) and ROI_{Ref1} (blue). The active region for the $FHOS>b$ contrast, ROI_{Act1}, covers a large part of the occipital lobe. (B) ROI_{Act2} (red) and ROI_{Ref2} (blue). The active region for the $F>HOS$ contrast, ROI_{Act2}, includes only parts of the inferior visual cortex that respond to faces. All ROIs are displayed overlaid on slices taken from a volume of the fMRI data set they were generated from.

where r_{RETRc} and r_{RETRr} stand for the cardiac and respiratory part of RETROICOR, respectively, and r_{CR} and r_{RVT} represent the CR and RVT regressors. The contributions of different regressors may then be estimated from these nested models and used to characterize the noise as in Ref. [9].

2.2.4. PCA-based analysis

This approach followed the methodology described in Ref. [10], with a few relevant modifications consisting of the following steps:

1. preprocessing of fMRI data as described in Section 2.2.1;
2. in *Rest* data sets, mapping of the correlation coefficient between the average signal time course of ROI_{Act1} or ROI_{Act2} and the remaining brain voxels;
3. definition of ROI_{Ref1} and ROI_{Ref2} by selecting all voxels with correlation coefficients above p_{cor}=50% of the maximum in each case (determined as the value yielding maximum average adjusted coefficient of determination, R^2_{adj}, values);
4. in *Loc* data sets, application of PCA to the voxel time courses in ROI_{Ref1} and ROI_{Ref2}, and selection of the 18 [10] eigenvectors associated to the largest eigenvalues in each case;
5. creation of 10 (determined in order to reduce processing time while maintaining acceptable statistical significance) additional vector sets obtained by randomizing the original PCA-derived eigenvectors, while preserving the original spectral power density (this was performed by taking the Fourier transform of each vector and replacing the phase of each complex Fourier component by a random value uniformly distributed between $-\pi$ and π);
6. orthogonalization of each the 10+1 eigenvector sets with respect to the localizer DM_0 regressor set;
7. creation of a PCA design matrix $DM_{PCA}=[DM_0^{Loc}\ r_{PCA}]$, where r_{PCA} contains the 18 orthogonalized PCA eigenvectors;
8. creation of 10 randomized (RND) design matrices $DM_{RND}=[DM_0^{Loc}\ r_{RND}]$, where r_{RND} represents each of 10 randomized versions of r_{PCA};
9. GLM analysis of *Loc* data using each of the created DM variants.

2.2.5. Outcome measures

In order to quantify the amount of signal information explained by a specific DM, the adjusted coefficient of determination, R^2_{adj}, and the percentage of variance explained, VE, were used [7]. Theoretically, R^2_{adj} is independent of the number of degrees of freedom (DOF) in the model, allowing for comparisons between different-sized models. Results were averaged across ROI_{Act1} for noise characterization because it was larger and more consistent across subjects than ROI_{Act2}; moreover, ROI_{Act2} is in general contained in ROI_{Act1}, and no important differences are expected between the two ROIs in terms of noise composition (i.e., the relative contributions from different physiological noise sources for total signal variance). Noise characteristics were evaluated in terms of sSNR and tSNR. The sSNR was calculated as the ratio between average signal intensity in ROI_{WM} and standard deviation in ROI_{BG}, averaged across time. No corrections for the Rayleigh noise distributions were applied as all values were in the high-SNR regime [26]. For computation of the tSNR, each voxel time course y in ROI_{Act1} of *Loc* data was initially fit to the base model, base model+PCA regressors or base model+PRs, and the resulting approximation y' was subtracted from the original signal y. The tSNR in each voxel was then calculated as the ratio between the mean and the standard deviation of $y–y'$, and these voxel-specific values were finally averaged across ROI_{Act1}.

Two measures of BOLD sensitivity were obtained: contrast estimation variance [27], averaged across ROI_{Act1} or ROI_{Act2}, and the number of active voxels (Z>2.3, cluster p<0.05).

For statistical testing, one-, two- or three-way analyses of variance (ANOVA) were used, with factors defined as *acquisition technique* (2D, 3D), *run type* (*Loc*, *Rest*) and *correction model* (DM_{RND}, DM_{PCA}, or DM_0, DM_6, depending on the type of approach). The significance threshold used was p<0.05.

3. Results

Activation analysis performed with the two functional contrasts revealed the expected anatomical locations in all subjects: the visual cortex for the global *FHOS>b* contrast and the face-specific cortical areas for the *F>HOS* contrast (consistent with reports in the literature [20]). This is illustrated for the 2D data of a single subject in Fig. 1, showing ROI_{Act1} and ROI_{Act2} as obtained with the localizer base model DM_0^{Loc}.

3.1. Physiological noise characterization

Physiological noise components were assessed in terms of their relative contributions to signal variance; the variance explained by each regressor set from the PR-based analysis is presented in Fig. 2. The “other” noise contributions include all contributions that are not captured in the used regressors, such as thermal noise fluctuation, spontaneous BOLD signal changes, subject motion and non-stable image artifacts. Both 2D-EPI and 3D-EPI show a significant contribution from physiological noise sources. From 2D to 3D, significant increases were observed in relative contributions from total physiological noise accompanied by decreases in relative contributions from “other” sources. Within physiological noise, RETROICOR contributions (cardiac and respiratory) increased significantly from 2D to 3D, while those from CR and RVT both decreased. The contribution of “other” sources to absolute variance can be estimated as follows: the noise percentage from “other” sources was 61% in 2D-EPI and 46% in 3D-EPI. The inverse of temporal SNR may serve as a noise measure when assuming that signal strength

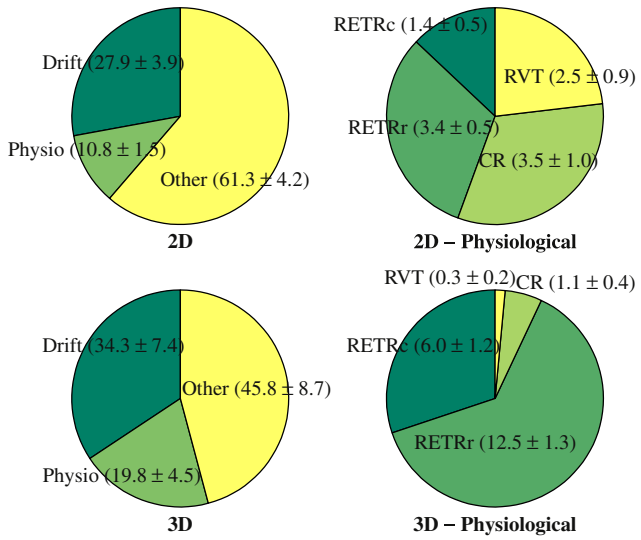

Fig. 2. Different noise contributions for fMRI signal information, expressed in terms of percentages of explained variance, from 2D and 3D *Rest* data. The results presented are averages across subjects (using ROI_{Act1}). Values in the pie sections state the relative contribution (in %) and the standard error over subjects.

remains constant. The tSNR obtained with base models was approximately 33 for 2D-EPI and 29 for 3D-EPI, resulting in a 16% higher variance from "other" noise sources in 2D-EPI relative to 3D-EPI.

3.2. Physiological noise correction

The outcome measures obtained for the full PR-based model (including all eight regressors) and the RND and PCA-based models, as well as for the base model DM_0, are presented in Fig. 3.

As expected, sSNR was significantly higher in 3D (86±8) than 2D (50±3) acquisitions. Although tSNR (Fig. 3A) was lower in 3D than 2D for the base model, it increased significantly with both PR- and PCA-based corrections. tSNR post-correction was higher for 3D than for 2D data, signifying that corrections were more effective in 3D data. This observation is supported by a significant interaction effect between *acquisition technique* and *correction model* in PCA analyses and the same trend for PR correction. As these values were obtained from the *Loc* data, residual stimulus-induced signal fluctuations may remain and

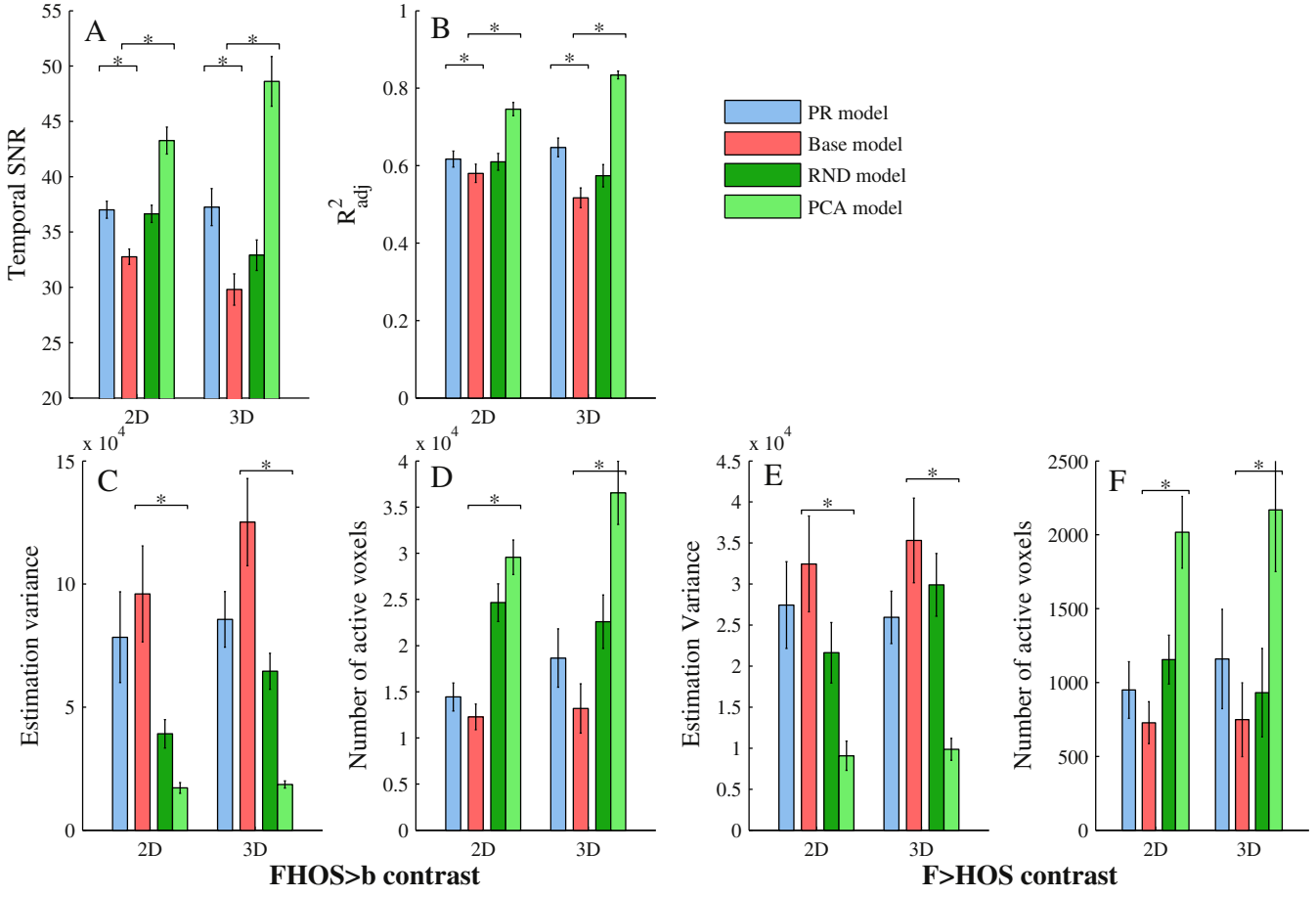

Fig. 3. PR- and PCA-based analysis results for tSNR, the adjusted coefficient of determination (R^2_{adj}), contrast estimation variance and number of active voxels (for either the *FHOS>b* contrast or the *F>HOS* contrast) obtained from 2D and 3D *Loc* data. Results are presented for base, full PR, RND and PCA linear models. The results presented are averages across subjects (using ROI_{Act1} for R^2_{adj} and tSNR, and ROI_{Act1} or ROI_{Act2} for contrast estimation variance); error bars represent the standard error. Significant main effects of each of the correction methods, PR or PCA based, are indicated with * ($p<0.05$).

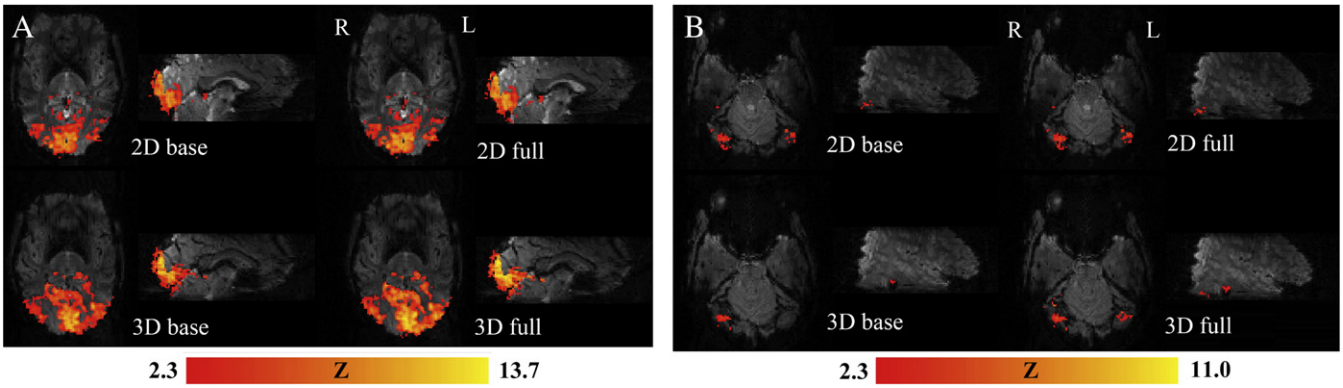

Fig. 4. An example of changes in Z statistic activation maps of 2D and 3D *Loc* data from a representative subject analyzed with base and PR-derived linear models, considering (A) an *FHOS>b* contrast or (B) an *F>HOS* contrast. Activation maps are shown overlaid on a volume of the data set from which they were generated. An axial slice (z=16 for *FHOS>b* or z=7 for *F>HOS*) and a sagittal slice (x=52 for *FHOS>b* or x=73 for *F>HOS*) are shown.

influence tSNR values, and although valid for comparisons, the numbers should be interpreted with some caution.

The information explained by each GLM, R^2_{adj} (Fig.3B), was significantly higher for both PR- and PCA-based models relative to the base model, in both 2D and 3D data. Importantly, PCA models, unlike RND models, explained significantly more information in 3D than in 2D. The R^2_{adj} values were similar between DM_0 and RND models, but were significantly different from those of PCA models. Because RND analyses have the same number of DOF as PCA analyses, but explain the data as well as the DM_0 analyses, the improvement observed from DM_0 to PCA models cannot be attributed to the decrease in DOF.

Analogous trends were observed in the analysis of BOLD sensitivity for the general visual contrast, *FHOS>b*, and the faces-specific contrast, *F>HOS* (Fig. 3C–F). These effects were statistically significant in the PCA-based analysis but not the PR-based analysis. The estimation variance of the base models (or the RND models in the PCA analysis) was higher in 3D than 2D, but the decreases observed from base to PR models and from RND to PCA models were such that both PR- and PCA-based models showed similar estimation variances for the two acquisition types. As expected, the estimation variance and number of active voxels obtained with the base model DM_0^{Loc} were different from those of RND models, which may be explained by the fact that these outcome measures do depend on the DOF in each linear model. The number of active voxels increased significantly from base to PR models and from RND to PCA models, and this increase was significantly larger in 3D than in 2D data, so that corrected 3D data showed more active voxels than corrected 2D data.

The trends observed in the sensitivity measures agree with the activation maps obtained for both contrasts, examples of which are presented in Fig. 4 (PR-based analysis) and Fig. 5 (PCA-based analysis). For the *FHOS>b* contrast, visual cortex activation is visible in all cases, but with higher *Z*-scores for 3D compared to 2D and for full compared to base models. Regarding the *F>HOS* contrast, activation of face-selective areas is detected in all cases — however, in the

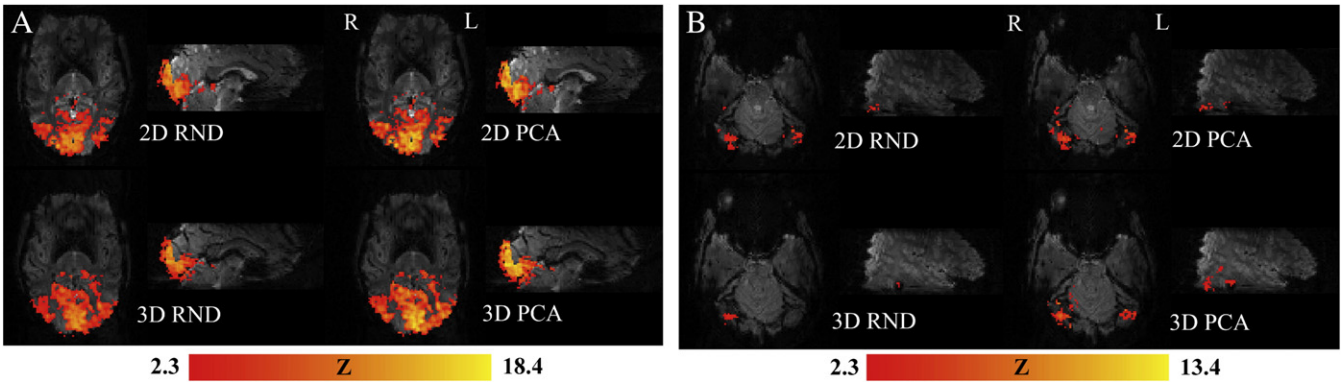

Fig. 5. An example of changes in Z statistic activation maps of 2D and 3D *Loc* data from a representative subject analyzed with RND and PCA-derived linear models, considering (A) an *FHOS>b* contrast or (B) an *F>HOS* contrast. Activation maps are shown overlaid on a volume of the data set from which they were generated. An axial slice (z=16 for *FHOS>b* or z=7 for *F>HOS*) and a sagittal slice (x=52 for *FHOS>b* or x=73 for *F>HOS*) are shown. The image quality of the 3D-EPI images is comparable to that of the standard 2D-EPI images. This is in agreement with recent publications on 3D-EPI ([14,15]) that report, among other characteristics, comparable Nyquist ghost levels for 2D and 3D-EPI data.

example shown, a cluster in the left occipital face-selective area can only be detected in 3D data after PR- or PCA-based correction. Specifically, as compared to PR model maps (Fig. 4), the corresponding PCA model maps (Fig. 5) show higher statistical significance.

4. Discussion

In this work, segmented 3D-EPI was compared to standard 2D-EPI in terms of the noise characteristics and efficiency of physiological noise removal in fMRI data acquired at 7 Tesla with both methods. Two physiological noise removal approaches were tested, both improving tSNR and BOLD sensitivity. One approach was based on physiological regressors derived from simultaneously acquired cardiac and respiratory signals, and the other relied on PCA of activation data using additional resting-state data. While it has already been shown that 3D-EPI provides advantages over 2D-EPI in a thermal-noise-dominated regime [14,15], in this study, benefits in the physiological-noise-dominated regime are demonstrated given appropriate correction.

The spatial resolution of $2\times2\times2mm^3$ used in this study is higher than the $3\times3\times3mm^3$ voxel size commonly used in fMRI at lower field strengths [28]. High resolution is beneficial at 7 Tesla because thick slices imply significant signal losses (especially for 2D-EPI) due to through-slice dephasing in regions with significant magnetic field gradients. On the other hand, the chosen voxel size reflects the higher spatial resolution achievable at 7 Tesla [29,30], while enabling nearly whole-brain coverage in a reasonable TR. As even close to $1mm^3$ resolution 7 Tesla data benefit from physiological noise removal [28], significant changes upon correction were expected for both 2D and 3D data in our case. In this study, it is shown that, upon correction, data from 3D acquisitions have superior BOLD sensitivity compared to 2D data in terms of estimation variance, number of active voxels and tSNR.

4.1. Physiological noise characterization

Our results show that relative physiological noise contributions increase from 2D to 3D data, while drift contributions remain fairly similar and other noise sources decrease. These findings are consistent with previous studies [15] indicating that, while image SNR is superior in 3D-EPI, physiological noise contributions also become more important and explain a larger fraction of total signal variance. It should be noted that the 2D results here obtained for PRs, although derived from R^2_{adj} values comparable in outcome to those of RND regressors, were in close agreement to those of a previous study [9] regarding the contributions from slow drift, physiological noise as a whole and other sources. For 3D-EPI, the PRs were significantly more effective at characterizing the noise than RND regressors, demonstrating that the PRs were valid data denoisers. Within physiological noise, it can be observed that RETROICOR components are in fact the only ones whose relative contributions increase from 2D to 3D, with those from CR and RVT becoming smaller. This observation suggests that the adopted 3D technique is specifically more sensitive to rapidly fluctuating noise from cardiac and/or respiratory phase-induced oscillations rather than to lower-frequency noise related to cardiac and/or respiratory rate fluctuations.

The high statistical significance of the interaction between *acquisition technique* and *correction model* for all measured variables related to BOLD sensitivity suggests that the physiological regressors used, particularly RETROICOR, were more effective in 3D, possibly due to its properties regarding slice timing differences: in 3D-EPI, each voxel signal can be considered to have originated almost solely from the time point in which the k_z=0 plane was acquired. Furthermore, the neighboring planes k_z=1 and −1, which have the highest energy, are acquired within 100ms and will have approximately the same cardiac and respiratory phase; hence, the same RETROICOR regressor is adequate for the whole volume. In contrast, in typical 2D-EPI acquisitions for fMRI, each slice is acquired at a significantly different time instant, thus theoretically requiring the use of slice-specific physiological regressors. This limitation becomes further complicated by the fact that the preliminary step of motion correction tends to distort slice acquisition times, thus requiring both effects to be accounted for simultaneously [31]. Note that neither of these observations is valid for segmented 2D-EPI, in which both neighboring *k*-space lines and neighboring slices are acquired distantly in time, resulting in further aliasing of the physiological signal fluctuations.

The inherently different acquisition strategies of 2D-EPI and 3D-EPI make it impossible to match all the acquisition parameters. In this study, the acquisition time per volume and brain coverage were kept constant, while the flip angle and TR were adapted for each sequence, as in previously reported experiments [14,15]. This meant that, while undersampling of cardiac and respiratory rates is equal for both sequences, the inflow of fresh spins may be different. However, the ROI chosen was contained mostly in central slices where inflow is expected to be minimal.

4.2. Physiological noise correction

Regarding the PCA- and PR-based approaches to noise correction, our results indicate that both methods improve the explaining power of linear models and their sensitivity to stimuli-induced neural activation. The PCA-based correction was found to be the most effective (with greater and statistically significant improvements in all detection sensitivity measures). This could be attributed to the more general nature of the PCA-based regressors, which are not limited to physiological noise related to the cardiac and respiratory function but can include any other vascular or neuronal coupling existing between the ROI and other brain regions. Differences observed between 2D and 3D results may be influenced to a certain extent by slice timing

differences — in the PR-based approach, due to the high-frequency nature of RETROICOR regressors, and in the PCA-based approach, due to the fact that spatial correlations of high-frequency noise become less evident between voxels of distant slices than between those of neighboring slices. Slice timing correction, as applied in 2D-EPI in this study, relies on fMRI signal interpolation to compensate for timing differences in slice acquisition. This commonly adopted measure [6,7,9,10], although not accounting for the deleterious effects of motion correction, has proved to be adequate for the time scale of signal contributions associated with typical stimulation paradigms. On the other hand, it should not be able to deal correctly with physiological signal fluctuations, as these are undersampled at typical fMRI TR values. In a previous study conducted with experimental 2D-EPI data processed with motion correction, followed by RETROICOR and slice timing correction or vice versa [31], the noise reduction efficacy of RETROICOR was found to decrease only by a small amount with timing errors introduced either by slice acquisition alone or by motion correction, thus suggesting that this issue may not play a major role in the trends observed.

The paradigm used in this work included the evaluation of a large brain region (the visual cortex, through the *FHOS* contrast) as well as a more restricted brain region (the face-specific areas of the visual cortex, through the *F>HOS* contrast). The fact that the results are consistent between regions suggests that the physiological noise removal should yield higher sensitivity in 3D-EPI over 2D-EPI in general, unrelated to the paradigm. Moreover, the fact that similar improvements in estimation variance and number of active voxels were obtained in both cases also indicates that the effectiveness of the adopted correction methods scales with ROI size and specificity — an aspect that is particularly important for the PCA-based approach, which strongly depends on the information provided by the "active" and "reference" ROIs.

While this study focused on the ability to characterize physiological noise in standard whole-brain functional data with an effective repetition time (>2 s) that is not able to accurately sample physiological noise, future work could be directed to the study of the implications of temporal acceleration of these techniques. Recently proposed multiplexed 2D-EPI [18] or 3D-EPI with acceleration on the parallel imaging in the *z*-direction [14] allow the reduction of the effective TR to less than 1s. The increased spatial resolution and associated reduction in SNR imply an overall reduction in physiological noise, although the decreased partial volume averaging may potentially increase the physiological noise in individual voxels. Together with its better temporal sampling, this will open new opportunities for correction methodologies.

4.3. Conclusion

Both the PR- and the PCA-based methods adopted for physiological noise correction were able to improve temporal SNR and BOLD sensitivity of segmented 3D-EPI to levels superior to those of corrected standard 2D-EPI, thus partially recovering the expected SNR advantages of 3D acquisitions. Hence, the 3D-EPI technique under study does have the potential to become a sensitive and useful tool for fMRI studies as long as its physiological noise-related limitations are adequately dealt with.

Acknowledgments

The authors would like to acknowledge Tobias Kober and Mayur Narsude for their help with the sequence implementation. This work was supported by Centre d'Imagerie BioMédicale (CIBM) of the UNIL, UNIGE, HUG, CHUV, EPFL and the Leenaards and Jeantet Foundations, and by the Portuguese Science Foundation (FCT) through Project PTDC/SAU-BEB/65977/2006 and ISR/IST plurianual funding through the PIDDAC Program funds.

References

[1] Edelstein WA, Glover GH, Hardy CJ, Redington RW. The intrinsic signal-to-noise ratio in NMR imaging. Magn Reson Med 1986;3:604–18.
[2] Krüger G, Kastrup A, Glover G. Neuroimaging at 1.5 T and 3.0 T: comparison of oxygenation-sensitive magnetic resonance imaging. Magn Reson Med 2001;45:595–604.
[3] Triantafyllou C, Hoge RD, Krueger G, Wiggins CJ, Potthast A, Wiggins GC, et al. Comparison of physiological noise at 1.5 T, 3 T, and 7 Tesla and optimization of fMRI acquisition parameters. Neuroimage 2005;26:243–50.
[4] Kruger G, Glover G. Physiological noise in oxygenation-sensitive magnetic resonance imaging. Magn Reson Med 2001;46:631–7.
[5] Glover GH, Li T-Q, Ress D. Image-based method for retrospective correction of physiological motion effects in fMRI: RETROICOR. Magn Reson Med 2000;44:162–7.
[6] Birn RM, Diamond JB, Smith MA, Bandettini PA. Separating respiratory-variation-related fluctuations from neuronal-activity-related fluctuations in fMRI. Neuroimage 2006;31:1536–48.
[7] Shmueli K, van Gelderen P, de Zwart JA, Horovitz SG, Fukunaga M, Jansma JM, et al. Low-frequency fluctuations in the cardiac rate as a source of variance in the resting-state fMRI BOLD signal. Neuroimage 2007;38:306–20.
[8] Cordes D, Haughton VM, Arfanakis K, Carew JD, Turski PA, Moritz CH, et al. Frequencies contributing to functional connectivity in the cerebral cortex in "resting-state" data. Am J Neuroradiol 2001;22:1326–33.
[9] Bianciardi M, Fukunaga M, van Gelderen P, Horovitz SG, de Zwart JA, Shmueli K, et al. Sources of functional magnetic resonance imaging signal fluctuations in the human brain at rest: a 7 Tesla study. Magn Reson Imaging 2009;27:1019–29.
[10] Bianciardi M, van Gelderen P, Duyn JH, Fukunaga M, de Zwart JA. Making the most of fMRI at 7 Tesla by suppressing spontaneous signal fluctuations. Neuroimage 2009;44:448–54.
[11] Petridou N, Schäfer A, Gowland P, Bowtell R. Phase vs. magnitude information in functional magnetic resonance imaging time series: toward understanding the noise. Magn Reson Imaging 2009;27:1046–57.
[12] Bodurka J, Ye F, Petridou N, Murphy K, Bandettini PA. Mapping the MRI voxel volume in which thermal noise matches physiological noise — implications for fMRI. Neuroimage 2007;34:542–9.
[13] Triantafyllou C, Hoge RD, Wald LL. Effect of spatial smoothing on physiological noise in high-resolution fMRI. Neuroimage 2006;32:551–7.

[14] Poser BA, Koopmans PJ, Witzel T, Wald LL, Barth M. Three dimensional echo-planar imaging at 7 Teslaesla. Neuroimage 2010;51: 261–6.
[15] van der Zwaag W, Marques JP, Kober T, Glover G, Gruetter R, Krueger G. Temporal SNR characteristics in segmented 3D-EPI at 7 Teslaesla. Magn Reson Med 2012;67:344–52.
[16] Feinberg DA, Reese TG, Wedeen VJ. Simultaneous echo refocusing in EPI. Magn Reson Med 2002;48(1):1–5.
[17] Moeller S, Yacoub E, Olman CA, Auerbach E, Strupp J, Harel N, Uğurbil K. Multiband multislice GE-EPI at 7 Teslaesla, with 16-fold acceleration using partial parallel imaging with application to high spatial and temporal whole-brain fMRI. Magn Reson Med 2010;63: 1144–53.
[18] Feinberg DA, Moeller S, Smith SM, Auerbach E, Ramanna S, Glasser MF, et al. Multiplexed echo planar imaging for sub-second whole brain FMRI and fast diffusion imaging. PLoS One 2010;5(12):1–11.
[19] Goerke U, Mölle H, Norris DG, Schwarzbauer C. A comparison of signal instability in 2D and 3D EPI resting-state fMRI. NMR Biomed 2005;18(8):534–42.
[20] Peelen M, Downing P. Within-subject reproducibility of category-specific visual activation with functional MRI. Hum Brain Mapp 2005;25:402–8.
[21] Sorger B, Goebel R, Schiltz C, Rossion B. Understanding the functional neuroanatomy of acquired prosopagnosia. Neuroimage 2007;35:836–52.
[22] Marques JP, Kober T, Krueger G, van der Zwaag W, de Moortele PF, Gruetter R. MP2RAGE, a self bias-field corrected sequence for improved segmentation and T1-mapping at high field. Neuroimage 2010;49:1271–81.
[23] Friston K, Holmes A, Worsley K, Poline J, Frith C, Frackowiak R. Statistical parametric maps in functional imaging: a general linear approach. Hum Brain Mapp 1995;2:189–210.
[24] Worsley KJ, Marret S, Neelin P, Vandal AC, Friston KJ, Evans AC. A unified statistical approach for determining significant signals in images of cerebral activation. Hum Brain Mapp 1996;4:58–73.
[25] Li C, Zheng C, Tai C. Detection of ECG characteristic points using wavelet transforms. IEEE Trans Biomed Eng 1995;42:21–8.
[26] Wiesskof RM. Simple measurement of scanner stability for functional NMR imaging of activation in the brain. Magn Reson Med 1996;36(4): 643–5.
[27] Woolrich MW, Ripley BD, Brady M, Smith SM. Temporal autocorrelation in univariate linear modelling of fMRI data. Neuroimage 2001;14:1370–86.
[28] Hutton C, Josephs O, Stadler J, Featherstone E, Reid A, Speck O, et al. The impact of physiological noise correction on fMRI at 7 Tesla. Neuroimage 2011;57:101–12.
[29] Yacoub E, Harel N, Ugurbil K. High-field fMRI unveils orientation columns in humans. Proc Natl Acad Sci USA 2008;105(30): 10607–12.
[30] van der Zwaag W, Francis S, Head K, Peters A, Gowland P, Morris P, et al. fMRI at 1.5, 3 and 7 Tesla: characterising BOLD signal changes. Neuroimage 2009;47(4):1425–34.
[31] Jones T, Bandettini P, Birn R. Integration of motion correction and physiological noise regression in fMRI. Neuroimage 2008;42:582–90.